

See discussions, stats, and author profiles for this publication at: <https://www.researchgate.net/publication/264231755>

The excited states of K₃ cluster: The molecular symmetry adapted non-adiabatic coupling terms and diabatic Hamiltonian matrix

ARTICLE in CHEMICAL PHYSICS · JUNE 2014

Impact Factor: 1.65 · DOI: 10.1016/j.chemphys.2014.05.022

CITATIONS

4

READS

58

2 AUTHORS, INCLUDING:

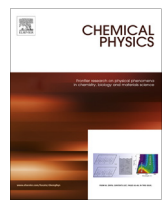


Saikat Mukherjee

Indian Association for the Cultivation of Sci...

10 PUBLICATIONS 25 CITATIONS

SEE PROFILE



The excited states of K_3 cluster: The molecular symmetry adapted non-adiabatic coupling terms and diabatic Hamiltonian matrix



Saikat Mukherjee, Satrajit Adhikari *

Department of Physical Chemistry & Raman Center for Atom, Molecule and Optical Sciences, Indian Association for the Cultivation of Science, Jadavpur, Kolkata 700 032, India

ARTICLE INFO

Article history:

Received 3 February 2014

In final form 28 May 2014

Available online 12 June 2014

Keywords:

K_3 cluster

Ab initio PESs

MS adapted NACTs

Diabatic Hamiltonian matrix

Dressed PECs

ABSTRACT

We calculate the adiabatic potential energy surfaces (PESs) and the non-adiabatic coupling terms (NACTs) for the excited electronic states of K_3 cluster by MRCI approach using MOLPRO. The NACTs are adapted with molecular symmetry to assign appropriate IREPs so that the elements of the Hamiltonian matrix are totally symmetric. We incorporate those NACTs into three-state adiabatic-to-diabatic transformation (ADT) equations to obtain ADT angles for constructing continuous, single-valued, smooth and symmetric diabatic Hamiltonian matrix, where its elements are fitted with analytic functions. Finally, we demonstrate that the *dressed diabatic* and *adiabatic-via-dressed diabatic* PECs show prominent topological effect over *dressed adiabatic* curves.

© 2014 Elsevier B.V. All rights reserved.

1. Introduction

The non-adiabatic coupling terms (NACTs) could play an important role [1–21] to understand the mechanism of spectroscopic and scattering problems with or without radiation-less charge transfer processes. One can handle those terms elegantly [1,4–13,17–21] to construct the so called “diabatic” (potentially coupled) Hamiltonian matrix instead of neglecting them forcefully for any arbitrary situation of interaction among the electronic states. Since the adiabatic potential energy surfaces (PESs) and the NACTs are unique and physically realizable, any formal development and its numerical implementation on beyond Born–Oppenheimer (BO) theory may naturally expected to start from the same representation (adiabatic PESs and NACTs). As the removable components of the NACTs are usually sharp functions of nuclear coordinates due to the singularities located at anywhere in the configuration space (CS), it is necessary to perform an unitary transformation from the kinetically coupled (adiabatic) Hamiltonian to the potentially (diabatic) one, where all the terms of the Hamiltonian would be continuous and smooth functions of nuclear coordinates and thereby, dynamical calculations could be accurate and stable.

The transformation from adiabatic to diabatic representation of SE for a given sub-Hilbert space is guaranteed to produce “correct” and “accurate” diabatic PESs under the following conditions: (a) The non-removable components of the NACTs are approximately zero [10]; (b) The vector fields created by the NACTs satisfy the so

called Curl Conditions [8,18]; (c) The *ab initio* calculated NACTs are adapted [17,21] with molecular symmetry [22,23] (MS) to assign their appropriate Irreducible Representations (IREPs) so that the nuclear Hamiltonian is totally symmetric under the operation of each element of the corresponding MS group of a molecule. In other words, when the diabatic PESs are continuous and single valued, the existence of a quantization rule [24] for removable components of the NACTs with singularities is predicted for a given sub-Hilbert space and such rule was confirmed [25] subsequently. Baer et al. carried out the beyond BO treatment for two state sub-Hilbert space and formulated [1] the diabatic Hamiltonian matrix in terms of adiabatic PESs and Adiabatic to Diabatic Transformation (ADT) angles. Sarkar et al. generalized [18] the BO treatment for any three/four coupled electronic states, where the explicit form of NACTs, Curl-Divergence equations and diabatic Hamiltonian matrix elements are derived in terms of ADT angles. This approach adapts [21] appropriate IREPs of the NACTs and paves a practical way to handle the NACTs with singularities at any point(s) or along a seam in the configuration space (CS) to construct continuous, single-valued, symmetric and smooth diabatic PESs.

Alkali trimers are well known for exhibiting the effect of Jahn–Teller (JT) and pseudo Jahn–Teller (PJT) interactions [26,27] in their spectral features. These clusters are convenient for theoretical calculation [28–38] to interpret the experimentally measured data [39–47] due to one-electron-valence configuration and few number of vibrational degrees of freedom (DOFs). As for example, Yarkony et al. confirmed [37] the presence of Conical Intersection (CI) at D_{3h} geometry in Li_3 cluster along with unusual CIs at C_{2v} points. de Vivie-Riedle et al. carried out [36] full configuration

* Corresponding author. Tel.: +91 33 2473 4971; fax: +91 33 2473 2805.

E-mail address: pcsa@iacs.res.in (S. Adhikari).

interaction calculation for ground as well as excited states of Na_3 cluster to generate PESs and transition dipole moment, and performed dynamics to reproduce experimental spectrum. Köppel et al. also simulated [32,34] the experimental spectra by using model Hamiltonian and showed the geometric phase effect [33,35] both under JT and PJT conditions on the same system. Koizumi and Bersuker extended [38] the PJT model Hamiltonian [30] and predicted four CIs between the excited $2^2\text{E}'$ states of the Na_3 cluster. We performed *ab initio* calculation for PESs and NACTs of $2^2\text{E}'$ and $1^2\text{A}'_1$ states of the same cluster with SA-CASSCF as well as MRCI level and confirmed six CIs between the $2^2\text{E}'$ states, where the three CIs [20] are at C_{2v} geometry and the other three CIs collapse [21] at the point of D_{3h} symmetry. The first theoretical calculation on K_3 was carried out [28] by Martins et al., where local spin density approximation on density functional theory was employed to calculate ground state PES as function of normal modes. The analytic fit of those adiabatic surfaces was made by Mead and Truhlar [29]. Woste et al. used the three photon ionization (TPI) technique and depicted [40] the Fourier spectrum of K_3 cluster at $\lambda = 798$ nm, but such experimental lines could not be assigned with its appropriate excited states. Ernst et al. investigated potassium doped Ar clusters by beam depletion (BD) and laser induced fluorescence (LIF) spectroscopy, and performed CASSCF level calculation to assign experimental spectrum of doublet potassium trimer. Such an investigation [43] found the one to one correspondence between experimental data and theoretical prediction for the states, $1^2\text{A}'_2$, $4^2\text{A}'_1$ and $3^2\text{B}'_2$. On the other hand, since the other low lying states ($1^2\text{E}'$, $2^2\text{E}'$, $1^2\text{A}'_1$, $2^2\text{A}'_1$ etc.) for K_3 are also interesting, there are multiple theoretical calculations even though the experimental predictions for those states are yet to be made. As for example, the potential energy curves (PECs) for the lowest twelve (12) doublet electronic states of K_3 were calculated by employing different *ab initio* methods and the couplings for JT-PJT interactions were discussed [45,46].

We perform *ab initio* calculation for the doublet states ($2^2\text{E}'$ and $1^2\text{A}'_1$) of K_3 cluster at the MRCI level to obtain the adiabatic PESs and the NACTs for those states. Since *ab initio* calculation by using any quantum chemistry package can assign IREPs to the adiabatic PESs, but not to the NACTs so far, it is theoretically and technically necessary to ensure that both the quantities adiabatic PESs and NACTs belong to appropriate IREPs in order to construct continuous, single-valued, symmetric and smooth diabatic PESs. We assign IREPs to the NACTs by adapting the MS group, where the generators of the character table of $D_{3h}(\mathbf{M})$ symmetry are tabulated by following the Longuet-Higgins [22] approach so that the diabatic Hamiltonian matrix is totally symmetric with respect to each symmetry element of the corresponding MS group. We employ our beyond Born–Oppenheimer theory for three state sub-Hilbert space of K_3 cluster, calculate ADT angles by plugging those IREPs adapted NACTs in ADT equations, construct diabatic Hamiltonian matrix elements by using adiabatic PESs and ADT angles, and such diabatic surfaces are accurately fitted with analytic functions. Since the present theoretical treatment and numerical implementation for the construction of diabatic PESs from adiabatic representation is enough accurate, it will be interesting to explore the topological effect in *dressed diabatic* and *adiabatic-via-dressed diabatic* curves over *dressed adiabatic* ones.

2. The theoretical background

2.1. Beyond Born–Oppenheimer theory for three-state sub-Hilbert space

The Born–Oppenheimer (BO) expansion [48,49] of the molecular wavefunction for a three-state electronic sub-Hilbert space and the total electron-nuclei Hamiltonian in the adiabatic representation are:

$$\begin{aligned}\Psi(s_e, s_n) &= \sum_{i=1}^3 \psi_i(s_n) \xi_i(s_e; s_n), \\ \hat{H} &= \hat{T}_{s_n} + \hat{H}_e(s_e, s_n), \\ \hat{T}_{s_n} &= -\frac{\hbar^2}{2} \sum_i \left(\frac{\nabla^2}{m_i} \right), \\ \hat{H}_e(s_e, s_n) \xi_i(s_e; s_n) &= u_i(s_n) \xi_i(s_e; s_n),\end{aligned}\quad (1)$$

where the nuclear and electronic coordinates are denoted by s_n and s_e , respectively, the expansion coefficients, $\psi_i(s_n)$ s, are actually the nuclear wavefunctions, the eigenfunctions and eigenvalues of the electronic Hamiltonian, $\hat{H}_e(s_e, s_n)$, are given by $\xi_i(s_e; s_n)$ and $u_i(s_n)$, respectively, and \hat{T}_{s_n} is the nuclear kinetic energy (KE) operator.

When the total electron-nuclear Hamiltonian and the BO expansion of the molecular wavefunction [Eq. (1)] are substituted into time independent SE [$\hat{H}\Psi(s_e, s_n) = E\Psi(s_e, s_n)$], the elements of non-adiabatic coupling matrices of the first [$\vec{\tau}^{(1)}$] and second [$\vec{\tau}^{(2)}$] kind are:

$$\vec{\tau}_{ij}^{(1)} = \langle \xi_i(s_e; s_n) | \vec{\nabla} \xi_j(s_e; s_n) \rangle, \quad (2a)$$

$$\vec{\tau}_{ij}^{(2)} = \langle \xi_i(s_e; s_n) | \nabla^2 \xi_j(s_e; s_n) \rangle, \quad (2b)$$

respectively. Since the matrices, $\vec{\tau}^{(1)}$ and $\vec{\tau}^{(2)}$ are related as:

$$\vec{\tau}^{(2)} = \vec{\tau}^{(1)} \cdot \vec{\tau}^{(1)} + \vec{\nabla} \vec{\tau}^{(1)}, \quad (3)$$

for a given sub-Hilbert space, we can arrive at the following compact form of kinetically coupled nuclear equations:

$$-\frac{\hbar^2}{2m} (\vec{\nabla} + \vec{\tau})^2 \psi + (U - E)\psi = 0, \quad (4)$$

with the following form of non-adiabatic coupling [$\vec{\tau} (\equiv \vec{\tau}^{(1)})$] and adiabatic PESs matrices:

$$\vec{\tau} = \begin{pmatrix} 0 & \vec{\tau}_{12} & \vec{\tau}_{13} \\ -\vec{\tau}_{12} & 0 & \vec{\tau}_{23} \\ -\vec{\tau}_{13} & -\vec{\tau}_{23} & 0 \end{pmatrix} \quad \text{and} \quad U = u_i \delta_{ij} \mathbf{I}, \quad (5)$$

respectively. For the same sub-Hilbert space, one can find a matrix (\mathbf{A}) to transform ($\psi = \mathbf{A}\psi^d$) the kinetically (adiabatic) coupled nuclear SE Eq. (4) to the potentially (diabatic) one:

$$-\frac{\hbar^2}{2m} \nabla^2 \psi^d + (W - E)\psi^d = 0, \quad W = \mathbf{A}^\dagger \mathbf{U} \mathbf{A} \quad (6)$$

under the condition:

$$\vec{\nabla} \mathbf{A} + \vec{\tau} \mathbf{A} = 0. \quad (7)$$

Such a condition is known as the Adiabatic to Diabatic Transformation (ADT) equation [6] and it has the following important theoretical and technical aspects:

- (i) Since the space of skew-symmetric (anti-symmetric) matrix ($N \times N$) form the Lie algebra of special orthonormal group ($SO(N)$), it is possible to find meaningful solution from Eq. (7) only when the chosen form of \mathbf{A} matrix satisfy orthonormality condition [$\mathbf{A}^\dagger \mathbf{A} = \mathbf{I}$] at any point in CS and show periodicity with respect to a parameter. Thus, the ADT matrix (\mathbf{A}) is supposed to be constituted with orthogonal basis and any operation under the rotation matrix (\mathbf{A}) should preserve the magnitudes and the angles between the functions, namely, Adiabatic PESs.
- (ii) The matrix equation for Adiabatic to Diabatic Transformation [Eq. (7)] involved with skew-symmetric matrix τ (NAC matrix) will generate path dependent solution (ADT angles) due to the choice of contour over the space coordinates, let say, ρ and ϕ . As the $SO(N)$ group is non-abelian, the rotation of an Euler or Euler like angle around an axis followed by

the rotation of that angle around another axis is different from the overall rotation in reverse order. In other words, the change of an ADT angle (known as pseudo Euler angle) due to the integration along a coordinate [ρ or ϕ] followed by its change with the integration along another coordinate [ϕ or ρ] is different from the overall change of ADT angle while performing the integration in reverse order. Such different paths of integration to obtain ADT angles lead to different ADT matrices and each of these ADT matrices will, therefore, be related with the others through orthogonal transformations [See Appendix B of Ref. 28]. If A_1 and A_2 are the two ADT matrices due to the choice of two different paths, the product between them for close contour takes the following form:

$$A_1^\dagger A_2 = A_1^\dagger(x_0, y_0) \exp(-\Delta x \Delta y (\text{Curl } \tau)_{xy}) A(x_0, y_0), \quad (8)$$

where x_0 and y_0 are the initial points and Δx and Δy are enough small increment on the contour. If the Curl of the NAC matrix is zero, both the chosen paths (even any) will produce same ADT matrices. Otherwise, for non zero Curl, the product matrix ($B = A_1 A_2$) is an orthogonal one as shown below:

$$\begin{aligned} B^\dagger B &= A_1^\dagger(x_0, y_0) \exp(\Delta x \Delta y (\text{Curl } \tau)_{xy}) \\ A(x_0, y_0) A_1^\dagger(x_0, y_0) \exp(-\Delta x \Delta y (\text{Curl } \tau)_{xy}) A(x_0, y_0) &= \mathbf{I}, \end{aligned} \quad (9)$$

which implies that the ADT matrices, A_1 and A_2 are related through an orthogonal transformation matrix, B .

- (ii) Since the model form of \mathbf{A} matrix has to be 3×3 for a three state sub Hilbert space, the orthonormality conditions demand the fulfillment of six relations. Thereby, three independent variables commonly called ADT angles, viz., Euler like angles of rotation [$\theta_{12}(s_n)$, $\theta_{23}(s_n)$ and $\theta_{13}(s_n)$], are the natural requirement to construct the three-state \mathbf{A} matrix by taking the product of three (3×3) rotation matrices, $\mathbf{A}_{12}(\theta_{12})$, $\mathbf{A}_{23}(\theta_{23})$, and $\mathbf{A}_{13}(\theta_{13})$ in different order, where one of them is shown in the *supplementary material*.

When the anti-symmetric form of τ [Eq. (5)] and the model form of \mathbf{A} [see Eq. (S.1) in *supplementary material*] matrices are substituted in ADT equation [Eq. (7)], Baer et al. [7] arrived to the following set of coupled differential equations for ADT angles:

$$\vec{\nabla}\theta_{12} = -\vec{\tau}^{12} + \tan\theta_{23}(\vec{\tau}^{13}\cos\theta_{12} - \vec{\tau}^{23}\sin\theta_{12}), \quad (10a)$$

$$\vec{\nabla}\theta_{23} = -(\vec{\tau}^{13}\sin\theta_{12} + \vec{\tau}^{23}\cos\theta_{12}), \quad (10b)$$

$$\vec{\nabla}\theta_{13} = -\frac{1}{\cos\theta_{23}}(\vec{\tau}^{13}\cos\theta_{12} - \vec{\tau}^{23}\sin\theta_{12}). \quad (10c)$$

On the contrary, if we substitute the different columns of \mathbf{A} matrix in Eq. (2a), the explicit form [18] of τ matrix elements in terms of ADT angles are obtained as:

$$\vec{\tau}_{12} = -\vec{\nabla}\theta_{12} - \sin\theta_{23}\vec{\nabla}\theta_{13}, \quad (11a)$$

$$\vec{\tau}_{23} = \sin\theta_{12}\cos\theta_{23}\vec{\nabla}\theta_{13} - \cos\theta_{12}\vec{\nabla}\theta_{23}, \quad (11b)$$

$$\vec{\tau}_{13} = -\cos\theta_{12}\cos\theta_{23}\vec{\nabla}\theta_{13} - \sin\theta_{12}\vec{\nabla}\theta_{23}. \quad (11c)$$

One can use Eqs. 11 to formulate the explicit form of Curl equation [18] for each NAC element in terms of ADT angles:

$$\text{Curl } \tau_{pq}^{12} = C_{12} = Z_{12} = -\cos\theta_{23}(\nabla_q\theta_{23}\nabla_p\theta_{13} - \nabla_p\theta_{23}\nabla_q\theta_{13}), \quad (12a)$$

$$\begin{aligned} \text{Curl } \tau_{pq}^{23} = C_{23} = Z_{23} = &\cos\theta_{12}\cos\theta_{23}(\nabla_q\theta_{12}\nabla_p\theta_{13} - \nabla_p\theta_{12}\nabla_q\theta_{13}) \\ &- \sin\theta_{12}\sin\theta_{23}(\nabla_q\theta_{23}\nabla_p\theta_{13} - \nabla_p\theta_{23}\nabla_q\theta_{13}) \\ &+ \sin\theta_{12}(\nabla_q\theta_{12}\nabla_p\theta_{23} - \nabla_p\theta_{12}\nabla_q\theta_{23}), \end{aligned} \quad (12b)$$

$$\begin{aligned} \text{Curl } \tau_{pq}^{13} = C_{13} = Z_{13} &= \sin\theta_{12}\cos\theta_{23}(\nabla_q\theta_{12}\nabla_p\theta_{13} - \nabla_p\theta_{12}\nabla_q\theta_{13}) \\ &+ \cos\theta_{12}\sin\theta_{23}(\nabla_q\theta_{23}\nabla_p\theta_{13} \\ &- \nabla_p\theta_{23}\nabla_q\theta_{13}) - \cos\theta_{12}(\nabla_q\theta_{12}\nabla_p\theta_{23} \\ &- \nabla_p\theta_{12}\nabla_q\theta_{23}), \end{aligned} \quad (12c)$$

where the Curl due to vector product of NACTs and analyticity of ADT matrix are defined as: $C_{ij} = (\boldsymbol{\tau}_q \boldsymbol{\tau}_p)_{ij} - (\boldsymbol{\tau}_p \boldsymbol{\tau}_q)_{ij}$ and $Z_{ij} = \frac{\partial}{\partial p} \boldsymbol{\tau}_q^{ij} - \frac{\partial}{\partial q} \boldsymbol{\tau}_p^{ij}$, respectively with $\nabla_p = \frac{\partial}{\partial p}$ and $\nabla_q = \frac{\partial}{\partial q}$. The Cartesian coordinates p and q denote nuclear DOFs.

- (iv) The components of the *ab initio* calculated NACTs are substituted in the set of coupled differential equations for ADT angles [Eq. (10)] and those stiff equations are solved by using Backward Differentiation Formula (BDF). Such angles and adiabatic PESs are substituted in the explicit form of the diabatic PES matrix elements [Eq. (S.2) in the *supplementary material*], where the cross derivatives of those angles [Eq. (12)] provide us the functional form of Curl condition over the CS to explore the existence of three state sub-Hilbert space.
- (v) Since the numerical values of the ADT angles are uniquely defined as the solution of ADT equation [Eq. (10)] for a chosen path, the Gimbal Lock like situation of ADT matrix (\mathbf{A}) will not appear for the construction of single-valued diabatic potential matrix. As for example, if we assume $\theta_{23} = \pi/2$, the ADT matrix turns into:

$$\mathbf{A} = \begin{pmatrix} \cos(\theta_{12} + \theta_{13}) & 0 & \sin(\theta_{12} + \theta_{13}) \\ -\sin(\theta_{12} + \theta_{13}) & 0 & \cos(\theta_{12} + \theta_{13}) \\ 0 & -1 & 0 \end{pmatrix}.$$

The transformation matrix (\mathbf{A}) will be same at a specific CS for infinitely different set of θ_{12} and θ_{13} values. On the contrary, the ADT equation will provide unique solution for ADT angles and thereby, the ADT matrix will be unique at each point of CS for a chosen path.

- (vi) Since it is necessary to transform the kinetically coupled adiabatic SE [Eq. (4)] to the potentially coupled diabatic one [Eq. (6)] to perform accurate and stable quantum dynamics, we wish to make sure before transformation all the terms of the Hamiltonian in the adiabatic representation are totally symmetric under the operation of each symmetry element of MS group, $D_{3h}(M)$ so that the diabatic PESs are continuous, single valued, symmetric and smooth at each point in the CS. Thereby, we need to assign appropriate IREPs of the NACT obtained from *ab initio* calculation before plugging those terms into ADT equation [Eq. (10)] to obtain the ADT angles for constructing the diabatic surfaces. Since the adiabatic PESs are the solution of electronic Hamiltonian by freezing the nuclear geometry at each grid point within the Born–Oppenheimer treatment, the point group symmetry can define the IREPs of those PESs. On the contrary, as the NACTs are calculated by considering the non rigidity of the nuclei, it is a necessity to assign the IREPs of those terms by MS adaptation for beyond Born–Oppenheimer treatment. We perform this adaptation separately because the *ab initio* quantum chemistry packages so far can not provide appropriate IREP adapted NACTs.

2.2. Molecular symmetry adaptation to the NACTs for the excited states of K_3 cluster

Calculations of adiabatic PESs by exploiting electronic structure theory (either by Hartree–Fock or post Hartree–Fock methods) implicitly consider BO approximation, where the nuclear geometries are freezed and thereby, point group symmetry can define

the IREPs of those surfaces. On the contrary, while calculating the NACTs to construct diabatic PESs, one need to consider the non rigidity of the molecule, i.e. to move on the Beyond BO regime. Since the point group can not assign the IREPs of those NACTs, the standard electronic structure packages do not provide any information on their symmetry except the magnitude. Thus, it is a necessity to consider higher symmetry operations that include feasible permutation-inversion of the nuclei and their rotation in the space to define the nodal patterns (IREPs) of NACTs, which is called molecular symmetry (MS) group of a molecule.

It should not be very surprising that whenever one deals with a molecule with several identical atoms, the permutation-inversion symmetry must play a key role in unraveling the complex spectra and dynamics of a molecule. In general, for any molecule which exhibits large amplitude motions, the notion of a point group is of limited utility and one needs to invoke a larger set of symmetries to account the molecular processes. On the other hand, all the elements of the *complete group of a Hamiltonian* [22] are not needed to take into account, because the time scale of a given laboratory experiment may be too short to allow certain nuclear permutations. Therefore, one can consider only the feasible transformation, which can be attained without passing over an ‘insuperable’ energy barrier, to constitute the molecular symmetry group. At present case, in K₃ cluster, the three shallow wells in the lower 2²E' PES are connected via the C_{2v} Cls with the upper 2²E' state at the barrier and thereby, the use of molecular symmetry operation for the permutation of the nuclei is appropriate.

Each symmetry operation \hat{O} of the MS group of a molecule transforms the vibronic modes, the three angles (Euler) to describe the orientations of a rigid body in a three dimensional Euclidean space and the permutation of nuclear spin. Therefore, one can express \hat{O} as a product of three different operations [23]:

$$\hat{O} = \hat{O}_a \hat{O}_b \hat{O}_c \quad (13)$$

where \hat{O}_a produces change in vibronic degrees of freedom (DOF), \hat{O}_b changes the Euler angles and \hat{O}_c permutes the nuclear spin. The following two important theorems [17] on MS group can relate the IREPs of a NACT for different nuclear coordinates as well as different NACTs for the same nuclear mode:

Theorem 1. When the IREP of an element of NAC matrix (say, τ_k^{ij}) between two electronic states i, j for a specific symmetry adapted nuclear coordinate s_l is assigned, the IREPs of the same element (τ_k^{ij}) for different nuclear coordinate s_k can be determined by the following relation:

$$\Gamma(\tau_k^{ij}) = \Gamma\left(\frac{\partial}{\partial s_k}\right) \times \Gamma\left(\frac{\partial}{\partial s_l}\right) \times \Gamma(\tau_l^{ij}), \quad (14)$$

where

$$\tau_k^{ij} = \langle \xi_i(s_e; s_n) | \frac{\partial}{\partial s_k} (\xi_j(s_e; s_n)) \rangle. \quad (15)$$

In the supplementary material, the possible four combinations for the IREPs of the NACTs are presented in detail. In order to select the correct combination from the four possible ones, we employ the quantization rule [24] Eq. (16) of the contour integrals over the NACTs evaluated along a closed loop L_g of nuclear coordinate s_n around a single CI:

$$\oint ds_n \cdot \tau(s_n | L_g) = \pm\pi. \quad (16)$$

Finally, the second combination gives non-zero residue for contour integral and thereby, seems to be the only feasible one.

Theorem 2. The second theorem considers a loop-type sequence of N molecular states with same spin multiplicity, say N doublet states for the K₃ cluster, D_a, D_b, D_c, ..., D_y, D_{z=a} and define a product ($\tau_k^{a,b}, \tau_k^{b,c}, \dots, \tau_k^{y,z=a}$):

$$\tau_k^{a,b,c,\dots,y,z=a} = \tau_k^{a,b} \tau_k^{b,c} \dots, \tau_k^{y,z=a}, \quad (17)$$

where the IREPs of different elements of the NAC matrix for a specific nuclear coordinate k are related as:

$$\begin{aligned} \Gamma(\tau_k^{a,b}) \times \Gamma(\tau_k^{b,c}) \times \dots \times \Gamma(\tau_k^{y,z=a}) &= \Gamma\left(\frac{\partial}{\partial s_k}\right)^N \\ &= \begin{cases} \Gamma\left(\frac{\partial}{\partial s_k}\right) & \text{when } N \text{ is odd} \\ A'_1 & \text{when } N \text{ is even and 1D IREP} \\ E' & \text{when } N \text{ is even and 2D IREP} \end{cases} \end{aligned}$$

The detail molecular symmetry adaptation for each element of the NACTs are given in the *supplementary material*. In Table 1, we present the IREPs for all the elements of NAC matrix in a compact form.

3. The adiabatic PESs and NACTs for the excited states of K₃ cluster

3.1. Ab initio calculation for PESs and NACTs

We calculate adiabatic PESs (2²E' and 1²A'_1) and NACTs among those states as functions of vibrational modes, bending (Q_x) and anti-symmetric stretching (Q_y) for a fixed value of symmetric stretching one ($Q_z = 4.4 \text{ \AA}$). The “breathing mode” Q_z preserves the D_{3h} symmetry, whereas Q_x and Q_y distort the D_{3h} equilateral triangle into a C_{2v} isosceles and a C_s scalene triangle, respectively. If the antisymmetric stretching coordinate, Q_y , is set to zero, the potential energy curves of 2²E' and 1²A'_1 symmetry turn into 2²A₁, 2²B₂ and 3²A₁ states at various non-zero values of Q_x . We have employed Pople split-valence double zeta 6-31++G** basis set [50] with (23s, 17p, 1d) / [6s, 5p, 1d] contraction scheme for K using EMSL Basis Set Library [51] in our MRCI level *ab initio* calculations by MOLPRO quantum chemistry package [52]. Since 2²E' and 1²A'_1 states of K₃ cluster are actually the 4th, 5th and 6th excited states of the system, the MRCI calculation is carried out with the first six (6) states, where those states are obtained by MCSCF approach involving the first 20 electronic states to attain the closest possible variational minimum with respect to the exact energies.

We have tabulated the energy values (in Hartree) of the first six electronic states of K₃ cluster at D_{3h} symmetry point ($Q_x = Q_y = 0$) in Table 2 and at one of the C_{2v} symmetry points ($Q_x \sim 0.05$, $Q_y \sim 0.001$, i.e. $\rho \sim 0.05 \text{ \AA}$ and $\phi = \pi/3$) in Table 3 considering various active space. It is clearly shown that the degeneracies of 1²E' and 2²E' states are best described for the four choices of active space, viz. (3, 11), (3, 12), (3, 13) and (3, 14). In Fig. 1, the energy difference between the 5th and 6th states is plotted (see the corresponding left axis) as a function of ρ for a fixed $\phi = \pi/3$ with the above four different active spaces. Such difference consistently tends to zero for those four active spaces, which confirms the existence of symmetry enforced CI at $\rho \rightarrow 0$ and accidental CI at $\rho \sim 0.05 \text{ \AA}$ with $\phi = \pi/3$. Similarly, the presence of other two accidental Cls at $\rho \sim 0.05 \text{ \AA}$ with $\phi = \pi, 5\pi/3$ can be demonstrated. We have also displayed the NACT between the 5th and 6th states (τ_5^{12}) at $\rho \rightarrow 0$ and $\rho \sim 0.05 \text{ \AA}$ ($\phi = \pi/3$) for the same four active spaces in Fig. 1 (attributed in the right axis). An intense observation of the figure reveals the convergence of the active spaces and thereby, the choice of active space for all *ab initio* calculations on this system is (3, 13) with optimum number of CSFs (728), where twenty-seven (27) orbitals are considered to be closed shell. Such calculation gives a minimum energy -1797.376578 Hartree at D_{3h} geometry for the ground state, 1²E'. The electronic structure calculations at D_{3h} and C_{2v} symmetry points of K₃ cluster for the dominant coefficients of the molecular orbitals also ensure the presence of symmetry enforced and

Table 1

Extended character table of molecular symmetry group $D_{3h}(M)$ with different NAC elements.

$D_{3h}(M)$	E	(123) (132)	(12) (13)	E^*	(123)* (132)*	(12)* (13)*	Coord.	deriv.	τ_k^{23}	τ_k^{12}
									τ_k	τ_k
A'_1	1	1	1	1	1	1			τ_ϕ	
A'_2	1	1	-1	1	1	-1	ϕ	$\frac{\partial}{\partial \phi}$		τ_ϕ
E'	2	-1	0	2	-1	0	x,y	$\frac{\partial}{\partial x}, \frac{\partial}{\partial y}$	τ_x, τ_y	τ_x, τ_y
A''_1	1	1	1	-1	-1	-1			τ_ρ	
A''_2	1	1	-1	-1	-1	1	ρ	$\frac{\partial}{\partial \rho}$		τ_ρ
E''	2	-1	0	-2	1	0				

Table 2

Single point energies (in Hartree) for different states with different active spaces at $Q_x = Q_y = 0$.

Active space	$1^2E'$	$1^2E'$	$1^2A''_2$	$2^2E'$	$2^2E'$	$1^2A''_1$
(3, 9)	-1797.376548	-1797.376515	-1797.356371	-1797.347591	-1797.347578	-1797.342650
(3, 10)	-1797.376570	-1797.376548	-1797.356435	-1797.347599	-1797.347596	-1797.342693
(3, 11)	-1797.376574	-1797.376574	-1797.356463	-1797.347600	-1797.347600	-1797.342708
(3, 12)	-1797.376576	-1797.376576	-1797.356495	-1797.347604	-1797.347604	-1797.342718
(3, 13)	-1797.376578	-1797.376578	-1797.356489	-1797.347611	-1797.347611	-1797.342716
(3, 14)	-1797.376582	-1797.376580	-1797.356502	-1797.347615	-1797.347614	-1797.342735
(3, 15)	-1797.376585	-1797.376581	-1797.356505	-1797.347620	-1797.347618	-1797.342737

Table 3

Single point energies (in Hartree) for $2^2E'$ states with different active spaces at $Q_x \sim 0.05$, $Q_y \sim 0.001$.

Active space	$2^2E'$	$2^2E'$
(3, 9)	-1797.347596	-1797.347588
(3, 10)	-1797.347604	-1797.347600
(3, 11)	-1797.347607	-1797.347607
(3, 12)	-1797.347609	-1797.347609
(3, 13)	-1797.347612	-1797.347612
(3, 14)	-1797.347612	-1797.347612
(3, 15)	-1797.347616	-1797.347614

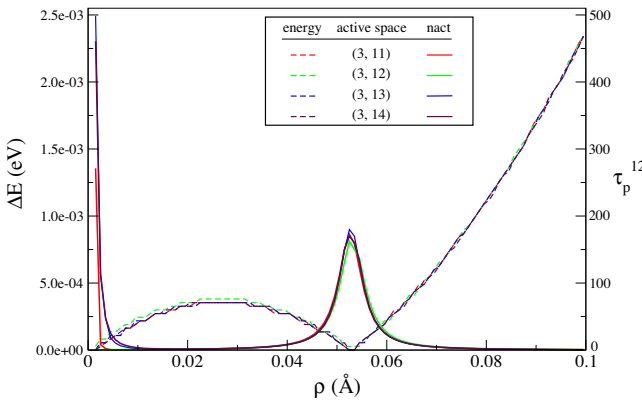


Fig. 1. Energy difference (ΔE) and the NACT of ρ component between the $2^2E'$ states for different active spaces.

accidental degeneracies at those points, respectively [see Section 3 of the supplementary material].

The one dimensional (1D) potential energy curves (PECs) for the six low lying states of K_3 cluster along the bending coordinate (Q_x) are calculated, where the antisymmetric and the symmetric stretching modes are fixed at $Q_y = 0$ and $Q_s = 4.4 \text{ \AA}$, respectively. Fig. 2(a) and (b) depict those curves as function of Q_x within the higher [-1.0 to 1.0] \AA and lower [-0.1 to 0.1] \AA ranges, respectively. Both these figures show that the curves are asymmetric as

function of Q_x as predicted elsewhere [45], i.e. the curves rise steeply for positive values of Q_x compared to its negative values. On the contrary, if we follow those curves with a denser grid of Q_x for its lower range [-0.1 to 0.1] \AA , it is quite interesting to observe that the $2^2E'$ states not only show degeneracy at $Q_x = 0.0 \text{ \AA}$ but also depict accidental degeneracy at $Q_x = -0.05 \text{ \AA}$.

Fig. 3 depicts the contour plots of PESs for $2^2E'$ and $1^2A'_1$, where the energies are scaled by subtracting the minimum energy of the lower $1^2E'$ state. We have used the so called numerical method (DDR) in MOLPRO to calculate the NACTs among $2^2E'$ and $1^2A'_1$ states over the range $\rho = 0.0$ to 0.1 \AA and $\phi = 0$ to 2π with a grid size (100×180) , where $\rho = \sqrt{Q_x^2 + Q_y^2}$ and $\phi = \tan^{-1} \frac{Q_y}{Q_x}$. Our calculations also show that apparently there are four (4) CIs between the $2^2E'$ states of K_3 system, where one of them is being located at $(Q_x, Q_y) = (0, 0)$ [$(\rho, \phi) = (0, 0)$] and the other three are at $\rho \approx 0.05 \text{ \AA}$, $\phi = \pi/3$, π and $5\pi/3$. Fig. 4 displays the ρ and ϕ components of NACTs as functions of normal mode coordinates $x(Q_x)$ and $y(Q_y)$.

3.2. The MS adaptation on NACTs

Since the determination of the IREP of an electronic wavefunction should be very difficult [17], if not even impossible by means of quantum chemistry and so it is for NACTs, we adapted them with MS group through the numerical implementation of the following two theorems: (a) **Theorem 1:** When the IREPs of the NACTs are known [see Table 1], the overall sign correction is performed for each of the NACTs according to the nodal patterns of the respective IREPs; (b) **Theorem 2:** The signs of τ_k^{13} and τ_k^{23} [$k = \rho, \phi$] are interchanged at the point of CIs. The upper panels (a, b) of Fig. 5 depict the numerical magnitude of τ_ρ^{ij} and τ_ϕ^{ij} (as obtained by using MOLPRO package) as function of ϕ for a fixed $\rho = 0.05 \text{ \AA}$, where the lower panels (c, d) display the IREP adapted (dotted line) ones with appropriate crossing due to CIs (solid line).

4. ADT angles (θ_{ij}) and their residues ($\bar{\theta}_{ij}^k$)

The MS adapted NACTs are substituted in ADT equations (Eqs. (10)) and those stiff differential equations are solved by using Backward Differentiation Formula over a 2D grid of geometries represented by 512×512 points in polar coordinates (ρ, ϕ) ranging

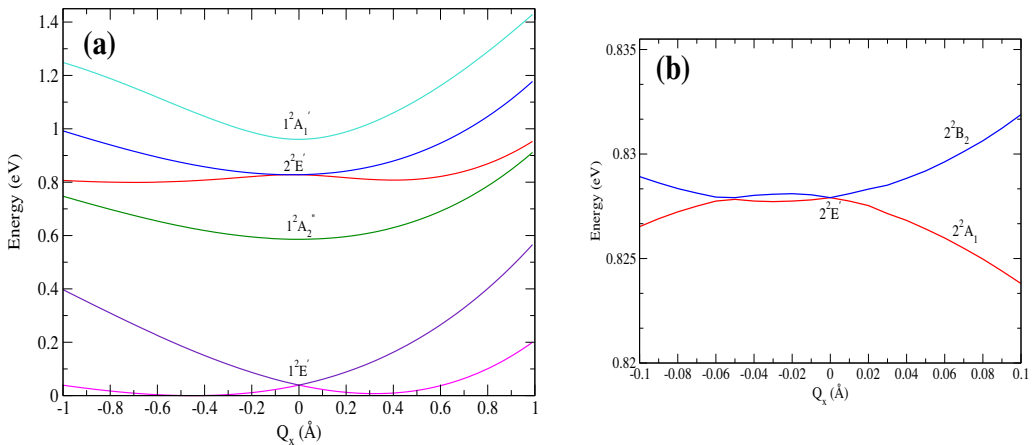


Fig. 2. (a): The 1D PECs (in eV) for the six lowest electronic states of K_3 cluster as a function of bending mode, (Q_x) with $Q_y = 0$ and $Q_s = 4.4 \text{ \AA}$; (b) The $2^2E'$ states depict the two CIs within the lower range [-0.1 to 0.1 Å].

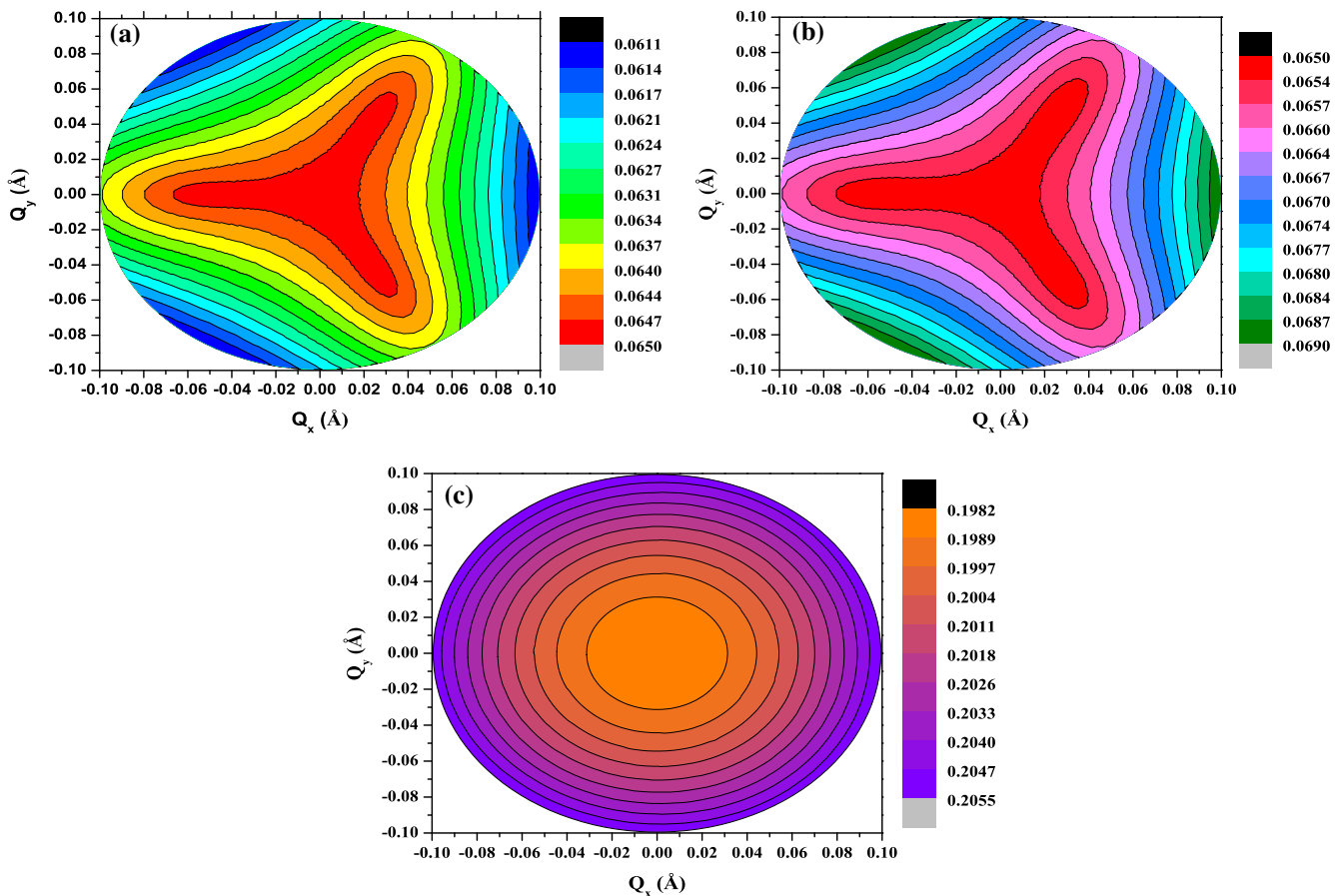


Fig. 3. Contour plot of the PESs in eV unit, where the surfaces at each point are scaled with the minimum energy of the ground state (-1797.376578 Hartree). Panels (a) and (b) display the lower and upper $2^2E'$ state and panel (c) shows $1^2A'_1$ state.

from $\rho = 0$ to 0.1 \AA and $\phi = 0$ to 2π to obtain the ADT angles. It is possible to integrate the two sets of coupled (ρ and ϕ) differential equations [Eqs. (10)] by choosing infinitely different paths and each path will generate different set of $\rho - \phi$ dependent ADT angles. Though the various sets of ADT angles obtained due to different choice of paths are expected to show gauge invariance, each set of such angles produces different ADT matrix and such matrices

will be related through orthogonal transformation [21] (See Section 2.1(ii)). At present case, we consider a rectangular path, where the differential equations for the ρ grid are integrated with positive increment from $\rho = 0$ to ρ_{max} for each positive step integration of the differential equations for the ϕ grid from 0 to 2π . The panels (a – c) of Fig. 6 depict the ADT angles [$\theta_{ij}(\rho, \phi)$] as functions of ρ and ϕ and the panels (a – c) of Fig. 7 present the residues of the

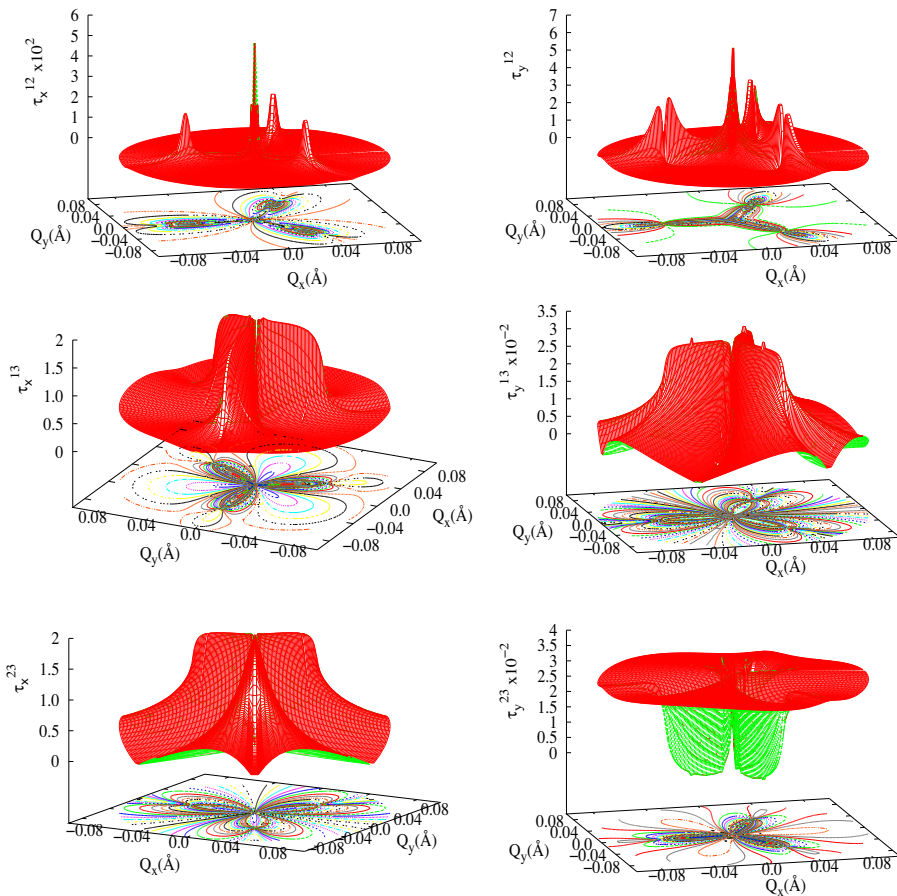


Fig. 4. The functional forms of the components of Non-Adiabatic Coupling (NAC) matrix elements as functions of Q_x and Q_y .

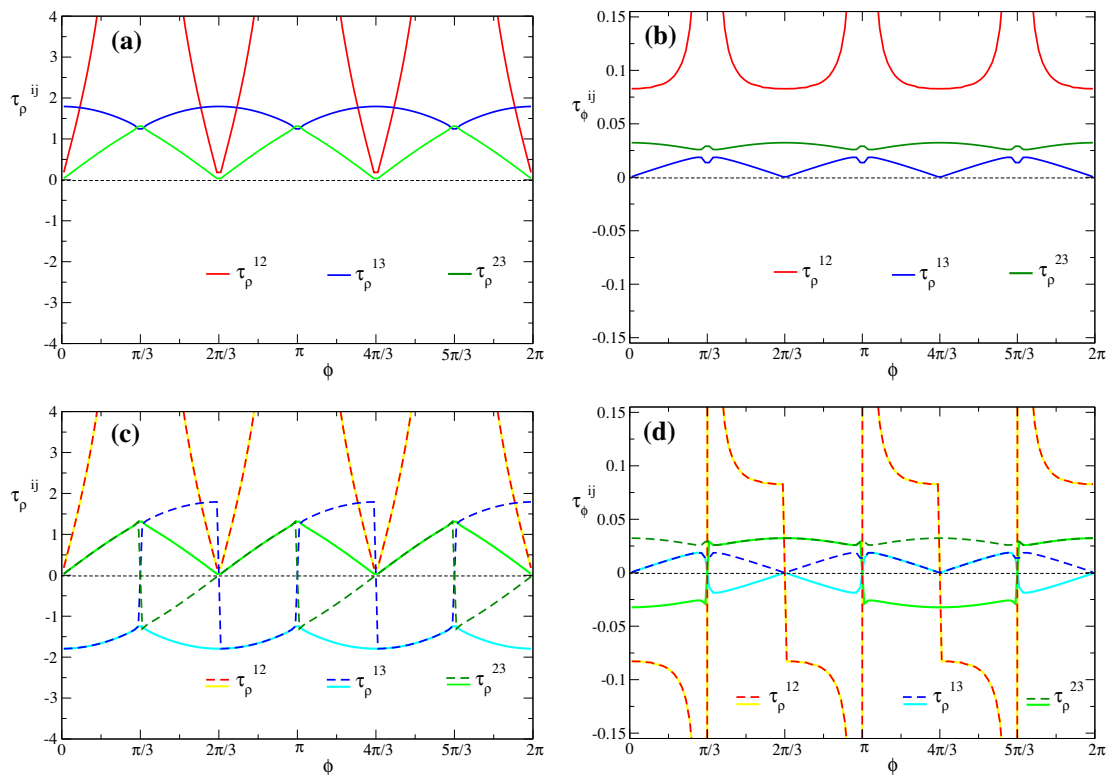


Fig. 5. Upper panels (a, b) show τ_p^{ij} vs. ϕ for a fixed $\rho = 0.05 \text{ \AA}$ before MS adaptation and lower panels (c, d) represent the same after MS adaptation.

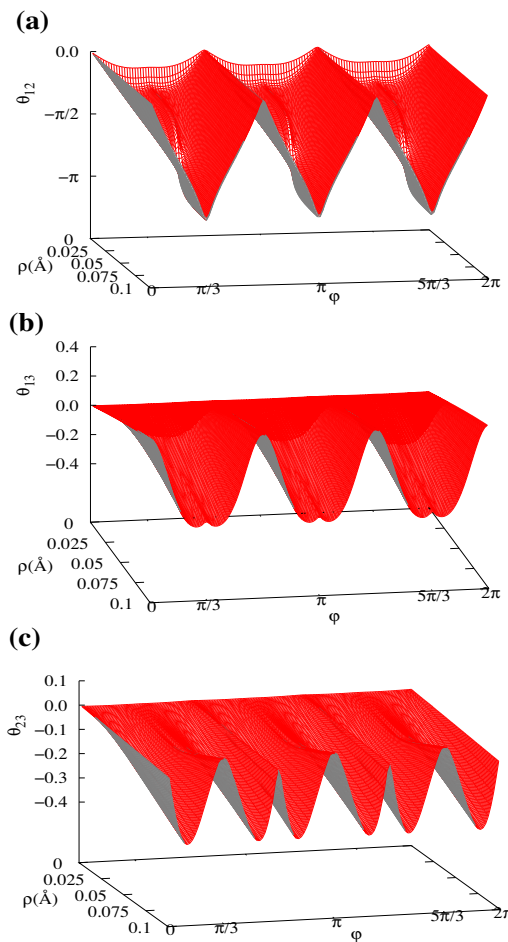


Fig. 6. The functional form of the ADT angles solved on a 2d contour integral.

ADT angles $[\bar{\theta}_{ij}^k = \int_0^{2\pi} \theta_{ij}(\rho_k, \phi) \cdot d\phi]$ as function of ρ . The panel (a) of Fig. 7 displays that the residue ($\bar{\theta}_{ij}^k$) for the ADT angle θ_{12} becomes close to 4π at asymptotic ρ and apparently predicts the presence of four CIs between the $2^2E'$ states located at $(Q_x, Q_y) = (0, 0)$ i.e. $(\rho, \phi) = (0, 0)$ and the other three are at $\rho \approx 0.05 \text{ \AA}$, $\phi = \pi/3, \pi$ and $5\pi/3$. Indeed, the number of peaks in the τ_{ρ}^{12} element in the CS [see Section 6 and Fig. 10(a)] and the number of sign changes in the functional form of diagonal elements of ADT (A_{11} or A_{22}) matrix [see Section 5 and Fig. 9(a)] endorse the existence of six CIs rather than four, where the three CIs collapse at D_{3h} point.

5. Curl condition ($\chi_{\text{Curl}\tau_{ij}}(\rho_k)$) and ADT matrix

A Curl Condition [8,18] has been formulated and proved to exist for each NACT ($\tilde{\tau}_{ij}$) of an isolated group of states (i.e. a sub-Hilbert space) by considering the analyticity of the ADT matrix (\mathbf{A}) for a pair of nuclear degrees of freedom (DOFs). The root mean square deviations (RMSDs) between the Mathematical (Z_{ij}) and ADT (C_{ij}) Curls employing the equation: $\chi_{\text{Curl}\tau_{ij}}(\rho_k) = \frac{1}{N} \sqrt{\sum_i^N (C_{ij}(\rho_k, \phi_i) - Z_{ij}(\rho_k, \phi_i))^2}$; $i, j = 1, 2, 3$ are calculated to explore the numerical validity of the Curl Condition. In order to display their difference more prominently, both the quantities, i.e. the Mathematical (Z_{ij}) and the ADT (C_{ij}) Curls are scaled by the maximum magnitude of either one of them. We calculate both the Curls for each NACT, evaluate the deviation between the two kind of Curls and then, add the square of such deviations along the ϕ coordinate to obtain the RMSDs as functions of ρ . Since the calculated RMSD values for τ_{12} appear as absolutely zero, the other two RMSDs for τ_{13} and τ_{23} are displayed in Fig. 8. The negligibly small magnitude of the RMSD as function of ρ describe the validity of the Curl Condition, namely, the existence of three excited state ($2^2E'$ and $1^2A'_1$) sub-Hilbert space for K_3 cluster.

Since the analytic expressions for the diagonal elements of the ADT matrix [53] of the JT CI model [54] for two state electron-nuclear Hamiltonian depict a single sign change along a contour around the CI point, such a property of a function was explored [4,5] and utilized for multi-states realistic model systems to find out the number of CIs and their locations in the CS. The *ab initio* calculated NACTs are adapted with appropriate IREPs to ensure that the adiabatic and finally, the diabatic Hamiltonians are totally symmetric w.r.t. MS group elements. While substituting those NACTs in ADT equations, we obtain the ADT angles and plug those angles in ADT matrix elements. At asymptotic ρ , the diagonal elements of ADT matrix, A_{11}/A_{22} show six sign changes in Fig. 9(a) and A_{33} displays no sign change in Fig. 9(b) as function of ϕ . These six sign changes indicate six CIs, where three are located at C_{2v} symmetry points ($\rho = 0.05 \text{ \AA}$ and $\phi = \pi/3, \pi$ and $5\pi/3$) and the other three collapse at the D_{3h} symmetry point ($\rho = 0$ and $\phi = 0$) [see Section 6].

6. Collapse of conical intersections at D_{3h} symmetry point

The interpretation on the collapse of CIs at D_{3h} point is based on the functional form of the amplitudes of $\tau_{\rho}^{12}(\rho, \phi)$ element. In order to find out the correctness of those amplitudes, we have explored the grid size dependence on the calculated amplitudes of τ_{ρ}^{12} element over the range, $0 \leq \rho \leq 0.01 \text{ \AA}$, where (a) the curves for τ_{ρ}^{12} are well converged with different grid size on the ρ coordinate at each specific ϕ value; (b) those profiles show different amplitudes

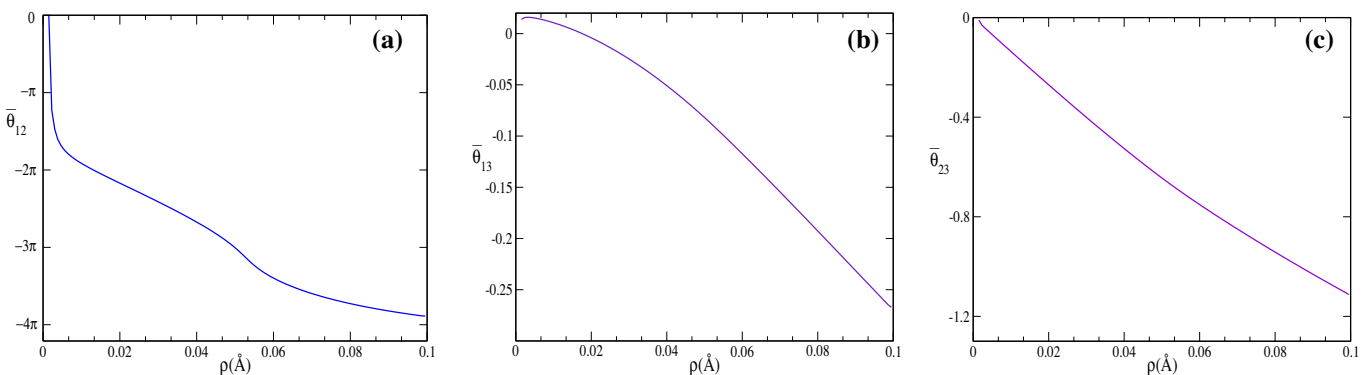


Fig. 7. The residues of the corresponding ADT angles $[\bar{\theta}_{ij}^k = \int_0^{2\pi} \theta_{ij}(\rho_k, \phi) \cdot d\phi]$ as function of ρ .

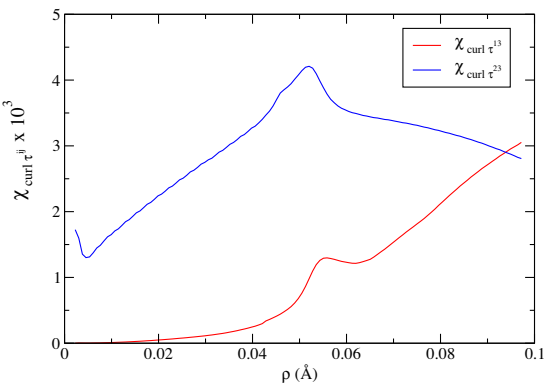


Fig. 8. RMSDs between Mathematical (Z_{ij}) and ADT (C_{ij}) curls for τ_{13} and τ_{23} .

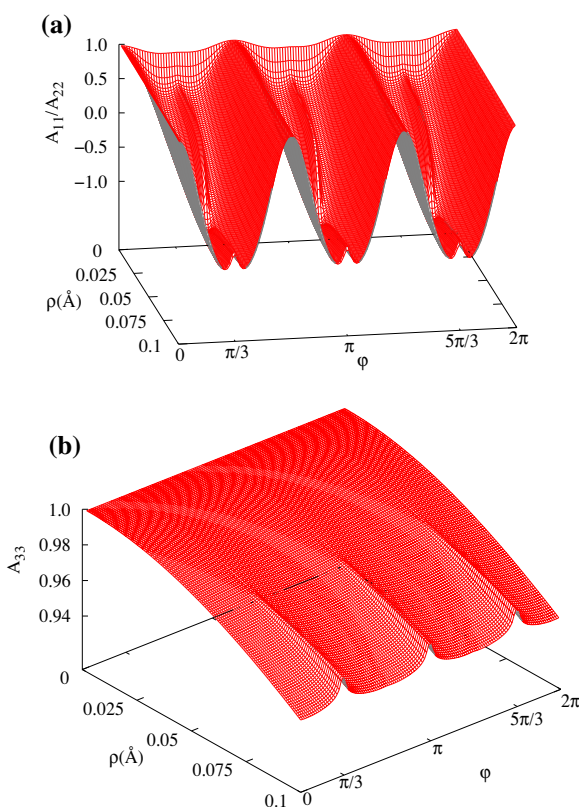


Fig. 9. The (1,1)/(2,2) and (3,3) elements of Adiabatic to Diabatic Transformation (ADT) matrix are shown.

as functions of ρ for different ϕ s (see Section 4 in the supplementary material).

Fig. 10(a) displays the spatial form of τ_ρ^{12} element as functions of ρ and ϕ , which clearly shows the position of six Cls in the CS. The three accidental Cls are located at C_{2v} symmetry points i.e. $\rho \approx 0.05 \text{\AA}$, $\phi = \pi/3$, π and $5\pi/3$, whereas the other three symmetry enforced Cls arise from very low values of ρ and eventually, collapse at the D_{3h} symmetry point located at $\rho = 0$, i.e. $(Q_x, Q_y) = (0,0)$. We are analyzing this issue in the following:

- We have manually removed the amplitudes from the functional form of τ_ρ^{12} element arising due to the three singularities for the accidental Cls at C_{2v} symmetry points to explore the effect of only those three Cls located around D_{3h} point. If the ADT equations are solved by employing such a modified τ_ρ^{12} element, the residue ($\bar{\theta}_{ij}^k$) for the ADT angle θ_{12} becomes

3π at large value of ρ ($\geq 0.1 \text{\AA}$) and predicts the presence of three symmetry enforced Cls at $\rho = 0$ between the $2^2E'$ states [see the solid line in Fig. 10(b)].

- In a similar fashion, we have suppressed those three singularities at very low ρ and considered τ_ρ^{12} element only with the other three singularities at C_{2v} symmetry points ($\rho \approx 0.05 \text{\AA}$, $\phi = \pi/3$, π and $5\pi/3$). When such a modified form of τ_ρ^{12} element is used to calculate the ADT angles, the corresponding residue for θ_{12} angle turns into 3π again at large value of ρ ($\geq 0.1 \text{\AA}$) and confirms the existence of three Cls at C_{2v} symmetry points [see the dotted line in Fig. 10(b)].

On the other hand, when we consider the τ_ρ^{12} element as it is obtained from *ab initio* calculation, the contributions of the ADT angle on the residue due to the Cls at $\rho = 0$ and $\rho \approx 0.05 \text{\AA}$ could be in different sign canceling each other and thereby, the residue becomes 4π instead of 6π . On the contrary, the sign change in the diagonal elements of the ADT matrix does not have such problems and clearly shows six sign changes [Fig. 9(a)], where each sign change indicates the presence of one Cl as predicted by Longuet-Higgins on Jahn-Teller model. In summary, since the three Cls at D_{3h} symmetry point [$(Q_x, Q_y) = (0,0)$] have collapsed into a single symmetry enforced Cl, the total contribution of the collapsed (apparently single) Cl at the D_{3h} point and the three accidental Cls at C_{2v} symmetry points on the residue ($\bar{\theta}_{12}^k$) becomes close to 4π [see Fig. 7(a)].

7. Diabatic PESs and fitting of the elements

When the adiabatic PESs and ADT matrix are substituted in Eq. (6) or ADT angles are incorporated in Eq. (S.2) of the supplementary material, the diabatic PESs are obtained as shown in Figs. 11 as functions of bending (Q_x) and antisymmetric stretching (Q_y) modes. The calculated diabatic surfaces are not only continuous and single valued but also smooth and symmetric. We present the analytic fitting of the elements of the diabatic PESs as functions of polar coordinate ($\rho = \sqrt{Q_x^2 + Q_y^2}$ and $\phi = \tan^{-1} \frac{Q_y}{Q_x}$) by using the singular value decomposition (SVD) methodology in least square sense [55] as given below:

$$W_{ii} = \alpha_0^{ii} + \beta^{ii} \rho^2 + \sum_n \sum_k a_{nk}^{ii} \rho^k \cos(3n\phi) + \sum_n \sum_k b_{nk}^{ii} \rho^k \sin(3n\phi); \\ i = 1, 2, 3. \quad (18a)$$

$$W_{ij} = \alpha_0^{ij} + \beta^{ij} \rho + \sum_n \sum_k a_{nk}^{ij} \rho^k \cos(3n\phi) + \sum_n \sum_k b_{nk}^{ij} \rho^k \sin(3n\phi); \\ i, j = 1, 2, 3 \quad (i < j), \quad (18b)$$

where the coefficients for those functions are presented in Tables 4–6. The parameters (α_0^{ij} , β^{ij} , a_{nk}^{ij} and b_{nk}^{ij}) in the analytic form of the diabatic matrix elements [Eq. (18)] and their fitted values [Tables 4–6] are assigned with appropriate units such that the PESs finally appear in eV. It is quite interesting to note that if we approximate Eq. (18) up to (i) the second term ($W_{ii} = \alpha_0^{ii} + \beta^{ii} \rho^2$ and $W_{ij} = \alpha_0^{ij} + \beta^{ij} \rho$), the diabatic PES matrix turns into the JT CI model [54], where the associated first two adiabatic PESs become degenerate at the D_{3h} symmetry point; (ii) the third and fourth terms only with $n = 1$ and $k = 1, 2, 3$, the surface matrix closely mimics the JT as well as PJT models [30,46], where the corresponding first two adiabatic PESs depict degeneracy not only at the D_{3h} symmetry point but also three accidental degenerate points at C_{2v} geometries.

8. Dressed adiabatic, dressed diabatic and adiabatic-via-dressed diabatic PECs: Topological effects

The dressed potentials are calculated employing the vib-rotational manifold obtained from each of the adiabatic and diabatic PESs. In order to explore the relevance of any PESs, Lipoff and

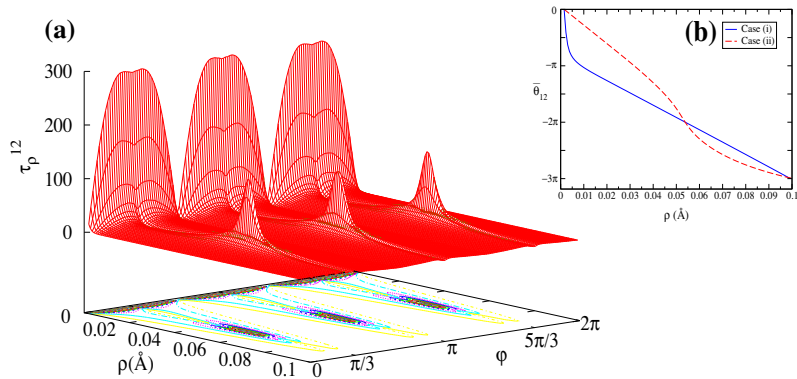


Fig. 10. (a) Functional form of τ_{ρ}^{12} as functions of ρ and ϕ ; (b) The residues of the ADT angle, $[\bar{\theta}_{12}^k]$ as function of ρ for the two cases are given in the inset.

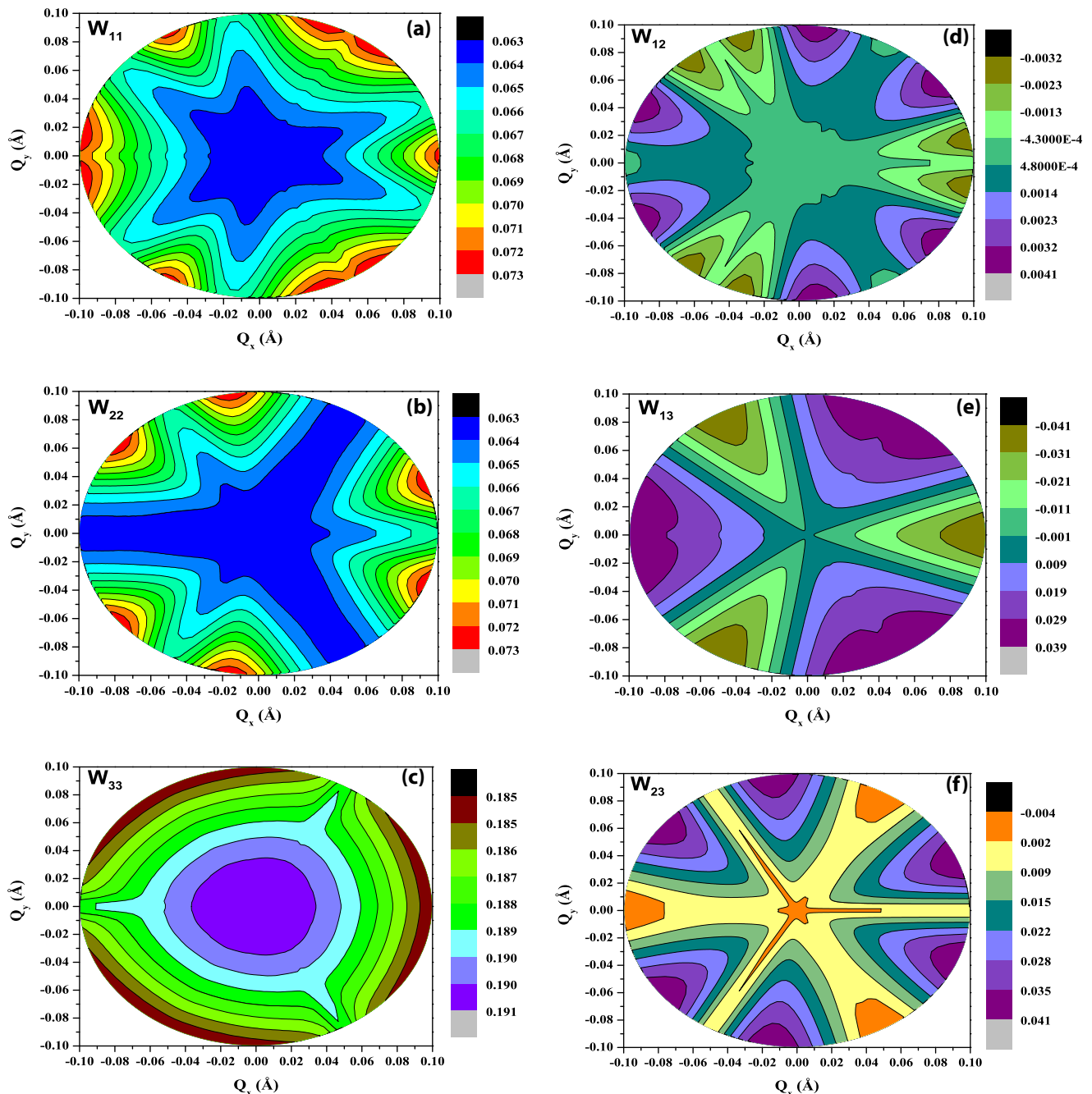


Fig. 11. The contour plots of diabatic PESs (eV) and the coupling elements (eV) are displayed as functions of normal modes.

Table 4

Parameters for the elements of diabatic surfaces.

	11	12	13	22	23	33
α_0^{ij}	0.062748	0.00	-0.000429	0.062747	0.000163	0.191232
β^{ij}	0.60	0.01	0.06	0.50	0.23	-0.40

Herschbach have proposed [56,57] this kind of study as a “blessed practice”. At present case, such dressed potentials are calculated by using vibrational (pseudo-rotational) eigenfunctions [58].

The three *dressed adiabatic* potentials, $u_i^a(\rho), i = 1, 2, 3$ are derived from the following expressions:

$$u_i^a(\rho) = \langle \xi_{i0}^a(\phi|\rho) | u_i(\phi|\rho) | \xi_{i0}^a(\phi|\rho) \rangle, \quad (19)$$

where $u_i(\phi|\rho)$ s are the three adiabatic PESs ($2^2E'$ and $1^2A'_1$) and $\xi_{i0}^a(\phi|\rho)$ s are the adiabatic pseudo-rotational (ϕ) ground eigenfunctions calculated for those surfaces. The normal modes Q_x and Q_y are related with the corresponding polar coordinates (ρ and ϕ) as:

$$\rho = \sqrt{Q_x^2 + Q_y^2} \text{ and } \phi = \tan^{-1} \frac{Q_y}{Q_x}.$$

On the other hand, the diabatic PESs and the corresponding pseudo-rotational ground eigenfunctions are defined by $W_{ii}(\phi|\rho)$ and $\xi_{i0}^d(\phi|\rho)$ ($i = 1, 2, 3$), respectively. The *dressed diabatic* PECs and the corresponding coupling terms are calculated as:

$$\tilde{W}_{ii}(\rho) = \langle \xi_{i0}^d(\phi|\rho) | W_{ii}(\phi|\rho) | \xi_{i0}^d(\phi|\rho) \rangle; i = 1, 2, 3, \quad (20a)$$

and

$$\tilde{W}_{ij}(\rho) = \langle \xi_{i0}^d(\phi|\rho) | W_{ij}(\phi|\rho) | \xi_{j0}^d(\phi|\rho) \rangle; i, j = 1, 2, 3 (i < j), \quad (20b)$$

where the *dressed diabatic* PEC matrix is defined as:

$$\tilde{\mathbf{W}}(\rho) = \begin{pmatrix} \tilde{W}_{11}(\rho) & \tilde{W}_{12}(\rho) & \tilde{W}_{13}(\rho) \\ \tilde{W}_{21}(\rho) & \tilde{W}_{22}(\rho) & \tilde{W}_{23}(\rho) \\ \tilde{W}_{31}(\rho) & \tilde{W}_{32}(\rho) & \tilde{W}_{33}(\rho) \end{pmatrix}. \quad (21)$$

While diagonalizing this matrix, the three *adiabatic-via-dressed diabatic* PECs, $u_i^d, i = 1, 2, 3$ are obtained. When the couplings among multiple electronic states are substantially small, the difference between the adiabatic and diabatic potential energy curves or surfaces are indistinguishable and thereby, the corresponding *dressed adiabatic*, *dressed diabatic* and *adiabatic-via-dressed diabatic* curves will also be close by. On the other hand, if those couplings are strong enough, the diabatic surfaces even cross at certain points in the CS and the adiabatic ones show avoided crossing at those points. Thus, it is difficult to follow these features of adiabatic and diabatic PESs as a function of many (nuclear) DOFs. In such situation, one can adopt the approaches, namely, *dressed adiabatic*, *dressed diabatic* and *adiabatic-via-dressed diabatic* to integrate out most of the spatial coordinates except one or two to see the topological effect prominently, if any, on the adiabatic surfaces.

The panels (a, b), (c, d) and (e, f) of Fig. 12 depict the *dressed adiabatic*, *dressed diabatic* and *adiabatic-via-dressed diabatic* PECs,

Table 5

Values of the a_{nk}^{ij} [$i, j = 1, 3$ ($i \leq j$)] terms.

n	k	W ₁₁	W ₁₂	W ₁₃	W ₂₂	W ₂₃	W ₃₃
1	1	-0.0090793459	-0.0003735221	-0.3481337549	0.0007002111	-0.0466541483	-0.0156406848
1	2	-0.0389671316	-0.3313965446	-0.2233550728	0.2018913816	1.1607438354	0.3035762467
1	3	-	1.0302069263	-	-	-	-2.4151667445
2	1	-0.0071428146	-0.0026124446	-0.0534671647	0.0038600198	-0.1026163256	-0.0149202126
2	2	0.2752281732	0.0502443681	-0.2695022978	-0.2903264938	-0.4639569424	0.2877697074
2	3	-	-1.3630034097	-	-	-	-1.2187455285
3	1	-0.0043423994	-0.0022293860	-0.0062429829	-0.0028161516	-0.0537741889	-
3	2	0.1276898215	0.0456135935	0.0506943888	-0.0440077954	0.1371339928	-
3	3	-	0.6185541644	-	-	-	-
4	1	-0.0032087693	-0.0015561464	-0.0003818073	-0.0010378396	-0.0164469285	-
4	2	0.0378894599	0.0988170935	-0.0362673017	-0.0237943051	-0.1459690254	-
4	3	-	-0.4467068755	-	-	-	-
5	1	-	-0.0004903811	-	-	-0.0189316456	-
5	2	-	-0.0027732019	-	-	0.0732616201	-
5	3	-	0.3765977597	-	-	-	-
6	1	-	-0.0005861646	-	-	-0.0046612884	-
6	2	-	0.0415427204	-	-	-0.0699258790	-
6	3	-	-0.2480182147	-	-	-	-

Table 6

Values of the b_{nk}^{ij} [$i, j = 1, 3$ ($i \leq j$)] terms.

n	k	W ₁₁	W ₁₂	W ₁₃	W ₂₂	W ₂₃	W ₃₃
1	1	0.0000544310	0.0000245001	-0.0000140299	-0.0000473191	-0.0000146663	-0.0000057392
1	2	-0.00008015838	-0.0009483439	-0.0000473113	0.0006253913	0.0004753989	0.0003670989
1	3	-	0.0080758139	-	-	-	-0.0021477340
2	1	-0.0000182107	-0.0000685736	0.0000359063	-0.0000178191	-0.0001098351	0.0000304372
2	2	0.0000769092	0.0023469172	0.0003065535	0.0001048997	0.0014985941	-0.0002438298
2	3	-	-0.0162241481	-	-	-	0.0011060944
3	1	0.0000667983	-0.0000161982	0.0001431340	-0.0000415529	0.0000695631	-
3	2	-0.0007389058	0.0007780634	-0.0005986087	0.0005700571	-0.0011302845	-
3	3	-	-0.0074559530	-	-	-	-
4	1	-0.0000193398	-0.0000555494	-0.0001232663	0.0000024687	0.0000003720	-
4	2	-0.0000398924	0.0021680165	0.0006384009	0.0001536225	0.0013936144	-
4	3	-	-0.0177463619	-	-	-	-
5	1	-	-0.0000172206	-	-	0.0000424877	-
5	2	-	0.0006495482	-	-	-0.0007080416	-
5	3	-	-0.0074885478	-	-	-	-
6	1	-	-0.0000181755	-	-	0.0000006724	-
6	2	-	0.0008780608	-	-	0.0007278649	-
6	3	-	-0.0065032762	-	-	-	-

respectively for $2^2E'$ and $1^2A'_1$ states. The splitting between the two $2^2E'$ states substantially changes from *dressed adiabatic* to *dressed diabatic* to *adiabatic-via-dressed diabatic* curves [see panels a, c, e]. Those two *dressed diabatic* curves are much closer than *dressed adiabatic* as well as *adiabatic-via-dressed diabatic* ones, where the topology of the lower E' state is completely reversed from *dressed adiabatic* to *adiabatic-via-dressed diabatic* state. Even the A'_1 state undergoes huge changes while performing the dressed calculation,

namely, the functional form of *dressed diabatic* state has the opposite gradient compared to *dressed adiabatic* state and finally, *adiabatic-via-dressed diabatic* state is also an increasing function compared to *dressed adiabatic* one, where the later attends a plateau at larger ρ compared to the former one [see b, e, f]. Indeed, it is important to observe that the third state ($1^2A'_1$) is even more affected while transforming the PES from *dressed adiabatic* to *dressed diabatic* to *adiabatic-via-dressed diabatic* PECs.

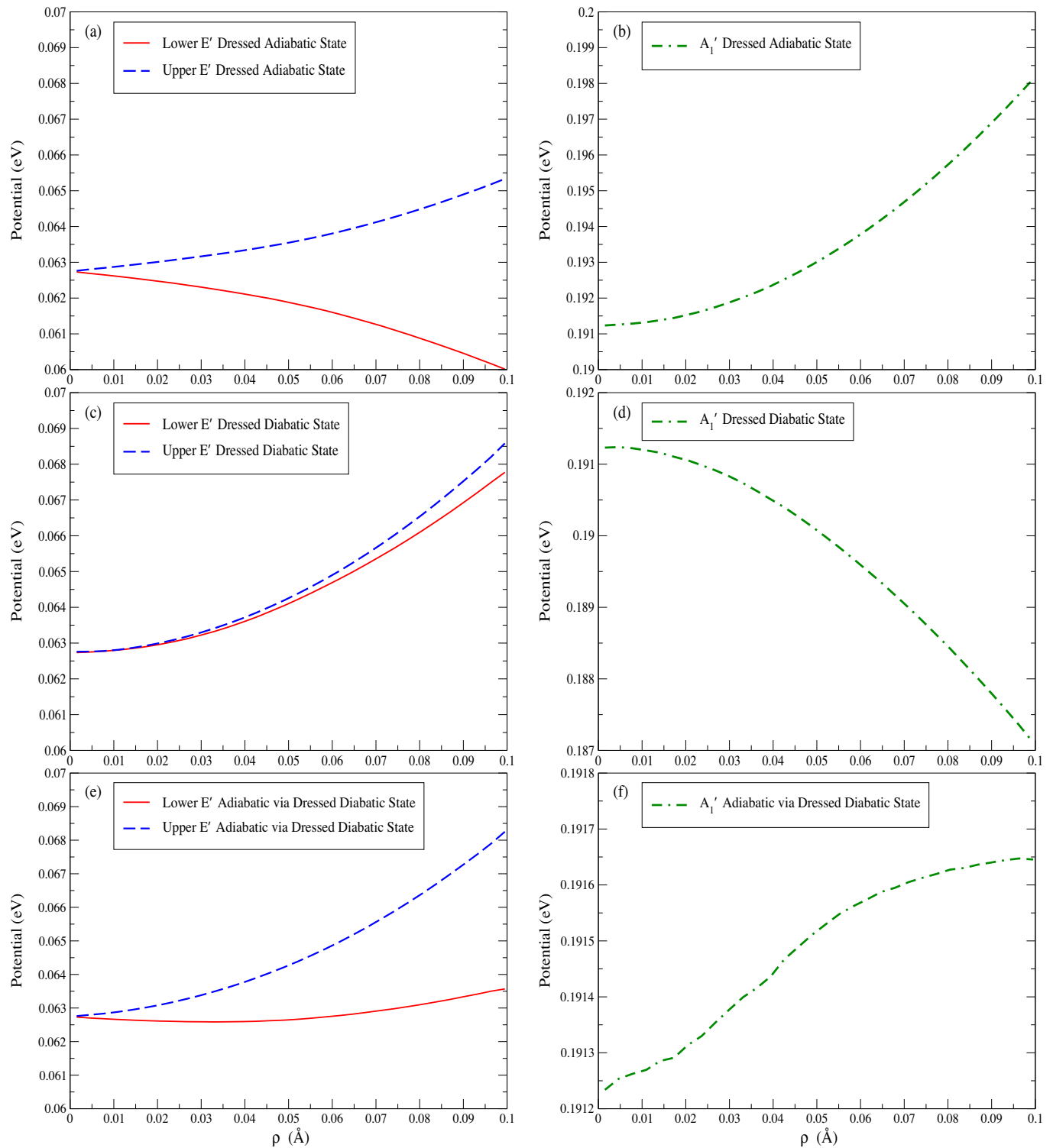


Fig. 12. *Dressed adiabatic*, *dressed diabatic* and *adiabatic-via-dressed diabatic* PECs for the two E' states are shown in panels a, c and e, whereas the same for A'_1 state are presented in panels b, d and f.

9. Summary

Since the adiabatic PESs and NACTs are physically meaningful and uniquely defined in the CS, it is important to work in the adiabatic representation for any theoretical development on beyond BO treatment and its application on molecular system. We have carried out *ab initio* calculation for adiabatic PESs and NACTs for the excited states ($2^2E'$ and $1^2A_1'$) of K_3 cluster by employing MRCI level methodology using quantum chemistry package MOLPRO and reproduced the existing potential energy curves [45]. As the NACTs could be singular at certain points in the CS, it is necessary to transform the kinetically coupled adiabatic SE to the potentially coupled diabatic ones, where the PESs would be continuous and smooth enough to perform accurate and stable quantum dynamics. Since we start with the adiabatic Hamiltonian for a molecular system/process, it is necessary to ensure that all its terms are totally symmetric w.r.t. the elements of the MS group designated for that system/process in order to construct symmetric, single-valued, continuous and smooth diabatic PESs. The adiabatic PESs are calculated within BO approximation, where any quantum chemistry package can assign their IREPs. On the contrary, as NACTs are calculated by using beyond BO treatment and the determination of the IREPs of electronic wavefunctions is difficult, such packages can not assign appropriate IREPs for NACTs. Therefore, we employ the MS to adapt the required IREPs for the NACTs before the Adiabatic to Diabatic Transformation is performed. The IREP adapted NACTs are substituted in ADT equation, the differential equations for the ADT angles (θ_{ij} s) are solved by invoking stiff equation solver technique [Backward Differentiation Formula (BDF)] over a 2D grid on normal modes, Q_x and Q_y ($\equiv \rho, \phi$) for a fixed Q_s , the validity of curl condition for the existence of three state sub-Hilbert space has been confirmed, and diabatic Hamiltonian matrix elements are constructed. The first two diagonal elements of the ADT matrix show six times sign changes within the domain of pseudo rotation (0 to 2π) and confirm the existence of six CIs between the two $2^2E'$ states, where the three CIs collapse at the D_{3h} symmetry point. Interestingly, the number of crossings along the seams between the diagonal elements of the diabatic PESs also confirm the number of CIs. Finally, while exploring the topological effect due to the non-adiabatic coupling terms, we have calculated the *dressed adiabatic*, *dressed diabatic* and *adiabatic-via-dressed diabatic* PECs, and found that the effect is quite prominent. Though there are multiple theoretical calculations including the present case on the low lying states of the K_3 cluster, the experimental measurement is yet to confirm those predictions.

Conflict of interest

The authors declare no competing financial interest and there are no conflict of interest.

Acknowledgments

SM acknowledges INSPIRE Programme (IF110026) of DST, INDIA for research fellowship. SA acknowledges BRNS, INDIA through project grants (sanction No. 2009/37/42/BRNS) for the research funding and IACS for CRAY supercomputing facility. The authors are grateful to Dr. Ankan Paul, Raman Center for Atomic, Molecular and Optical Sciences, IACS and his students for the fruitful discussion on electronic structure calculation.

Appendix A. Supplementary data

Supplementary data associated with this article can be found, in the online version, at <http://dx.doi.org/10.1016/j.chemphys.2014.05.022>.

References

- [1] R. Baer, D. Charutz, R. Kosloff, M. Baer, J. Chem. Phys. 105 (1996) 9141.
- [2] A.J.C. Varandas, Z.R. Xu, J. Chem. Phys. 112 (2000) 2121.
- [3] S. Adhikari, G.D. Billing, J. Chem. Phys. 111 (1999) 40.
- [4] M. Baer, S.H. Lin, A. Allijah, S. Adhikari, G.D. Billing, Phys. Rev. A 62 (2000) 32506.
- [5] S. Adhikari, G.D. Billing, A. Allijah, S.H. Lin, M. Baer, Phys. Rev. A 62 (2000) 32507.
- [6] M. Baer, Chem. Phys. Lett. 35 (1975) 112.
- [7] Z.H. Top, M. Baer, J. Chem. Phys. 66 (1977) 1363.
- [8] M. Baer, Beyond Born – Oppenheimer: Conical Intersections and Electronic Nonadiabatic Coupling Terms, Wiley – Interscience, 2006.
- [9] C.A. Mead, D.G. Truhlar, J. Chem. Phys. 77 (1982) 6090.
- [10] N. Matsunaga, D.R. Yarkony, Mol. Phys. 93 (1998) 79.
- [11] R.G. Sadygov, D.R. Yarkony, J. Chem. Phys. 109 (1998) 20.
- [12] B.K. Kendrick, C.A. Mead, D.G. Truhlar, Chem. Phys. 277 (2002) 31.
- [13] R. Abril, A. Kuppermann, J. Chem. Phys. 116 (2002) 1035.
- [14] W. Domcke, D.R. Yarkony, H. Koppel (Eds.), Conical Intersections: Electronic Structure, Dynamics & Spectroscopy, World Scientific, 2004.
- [15] W. Domcke, D.R. Yarkony, Annu. Rev. Phys. Chem. 63 (2012) 325.
- [16] D.R. Yarkony, Chem. Rev. 112 (2012) 481.
- [17] S. Al-Jabour, M. Baer, O. Deeb, M. Leibscher, J. Manz, X. Xu, S. Zilberg, J. Phys. Chem. A 114 (2010) 2991.
- [18] B. Sarkar, S. Adhikari, J. Chem. Phys. 124 (2006) 074101.
- [19] A.K. Paul, S. Sardar, B. Sarkar, S. Adhikari, J. Chem. Phys. 131 (2009) 124312.
- [20] A.K. Paul, S. Ray, D. Mukhopadhyay, S. Adhikari, J. Chem. Phys. 135 (2011) 034107.
- [21] S. Mukherjee, S. Bandyopadhyay, A.K. Paul, S. Adhikari, J. Phys. Chem. A 117 (2013) 3475.
- [22] H.C.L. Higgins, Mol. Phys. 6 (5) (1963) 445.
- [23] P.R. Bunker, P. Jensen, Molecular Symmetry and Spectroscopy, second ed., National Research Council of Canada, 2006.
- [24] M. Baer, J. Phys. Chem. A 104 (2000) 3181.
- [25] D.R. Yarkony, J. Chem. Phys. 105 (1996) 10456.
- [26] I.B. Bersuker, The Jahn-Teller Effect, Cambridge University Press, 2006.
- [27] R. Englman, The Jahn-Teller Effect in Molecules and Crystals, Wiley – Interscience, New York, 1972.
- [28] J.L. Martins, R. Car, J. Buttet, J. Chem. Phys. 78 (1983) 5646.
- [29] T.C. Thompson, G. Izmirlian Jr., S.J. Lemon, D.G. Truhlar, C.A. Mead, J. Chem. Phys. 82 (1985) 5597.
- [30] F. Coccini, T.H. Upton, W. Andreoni, J. Chem. Phys. 88 (1988) 6068.
- [31] F. Spiegelmann, D. Pavolini, J. Chem. Phys. 89 (1988) 4954.
- [32] R. Meiswinkel, H. Köppel, Chem. Phys. 144 (1990) 117.
- [33] J. Schön, H. Köppel, J. Chem. Phys. 103 (1995) 9292.
- [34] M. Mayer, L.S. Cederbaum, H. Köppel, J. Chem. Phys. 104 (1996) 8932.
- [35] J. Schön, H. Köppel, J. Chem. Phys. 108 (1998) 1503.
- [36] R. de Vivie-Riedle, J. Gaus, V. Bonačić-Koutecký, J. Manz, B. Reischl-Lenz, P. Saalfrank, Chem. Phys. 223 (1997) 1.
- [37] R.G. Sadygov, D.R. Yarkony, J. Chem. Phys. 110 (1999) 3639.
- [38] H. Koizumi, I.B. Bersuker, Phys. Rev. Lett. 83 (1999) 3009.
- [39] G. Delacrétaz, E.R. Grant, R.L. Whetten, L. Wöste, J.W. Zwanziger, Phys. Rev. Lett. 56 (1986) 2598.
- [40] H. Ruppe, S. Rutz, E. Schreiber, L. Wöste, Chem. Phys. Lett. 257 (1996) 356.
- [41] J. Higgins, C. Callegari, J. Reho, F. Stienkemeier, W.E. Ernst, K.K. Lehmann, M. Gutowski, G. Scosse, Science 273 (1996) 629.
- [42] W.E. Ernst, O. Golonka, Phys. Scr. T112 (2004) 27.
- [43] J. Nagl, A.W. Hauser, A.G.C. Callegari, W.E. Ernst, J. Phys. Chem. A 111 (2007) 12386.
- [44] J. Nagl, G. Auböck, A.W. Hauser, O. Allard, C. Callegari, W.E. Ernst, Phys. Rev. Lett. 100 (2008) 063001.
- [45] A.W. Hauser, C. Callegari, P. Soldan, W.E. Ernst, J. Chem. Phys. 129 (2008) 044307.
- [46] A.W. Hauser, C. Callegari, P. Soldan, W.E. Ernst, Chem. Phys. 375 (2010) 73.
- [47] A.W. Hauser, W.E. Ernst, Phys. Chem. Chem. Phys. 13 (2011) 18762.
- [48] M. Born, J.R. Oppenheimer, Ann. Phys. (Leipzig) 84 (1927) 457.
- [49] M. Born, K. Huang, Dynamical Theory of Crystal Lattices, Oxford University Press, Oxford, 1954.
- [50] V.A. Rassolov, J.A. Pople, M.A. Ratner, T.L. Windus, J. Chem. Phys. 109 (1998) 1223.
- [51] D. Feller, J. Comput. Chem. 17 (1996) 1571.
- [52] H.-J. Werner, P.J. Knowles, G. Knizia, F.R. Manby, M. Schütz et al., Molpro, version 2010.1, a package of ab initio programs, 2010. see <<http://www.molpro.net>>.
- [53] G. Herzberg, H.C.L. Higgins, Discuss. Faraday Soc. 35 (1963) 77.
- [54] H.A. Jahn, E. Teller, Proc. R. Soc. (London) 161 (1937) 220.
- [55] W.H. Press, S.A. Teukolsky, W.T. Vetterling, B.P. Flannery, Numerical Recipes in FORTRAN, Cambridge University Press, 1992.
- [56] S.H. Lipoff, D.R. Herschbach, Mol. Phys. 108 (2010) 1133.
- [57] D.R. Herschbach, Faraday Discuss. 142 (2009) 9.
- [58] A. Csehi, A. Bende, G.J. Halász, A. Vibók, A. Das, D. Mukhopadhyay, S. Mukherjee, S. Adhikari, M. Baer, J. Phys. Chem. A. <[10.1021/jp412738s](http://dx.doi.org/10.1021/jp412738s)>.